Original Research Article

Effects of Airfoil Geometry on Lift Generation: A Computational Fluid Dynamics Study of NACA Airfoils

Patrick Louden

Eastside Preparatory School, 10613 NE 38th Place, Kirkland, WA 98033, United States

ABSTRACT

Airfoil geometry plays a significant role in lift generation and wing performance. Many of its effects have already been theorized through thin-airfoil theory and tested in specific applications. However, there have been few papers with a unified framework to examine the effects of different aspects of airfoil geometry across multiple angles of attack and Reynolds numbers, leading to a lack of concrete information on their relative influences on aerodynamic performance. In this study, four different NACA airfoils with varying cambers, thicknesses, and maximum camber locations were tested using computational fluid dynamics in Ansys Fluent. These airfoils were rotated from 0° to 20° angle of attack in a transient simulation, with data taken every 0.8° starting at 0.8°, at four Reynolds numbers ranging from 1,044,521 to 73,116,483, while recording the coefficient of lift vs. angle of attack curves. Increasing the camber relative to the NACA 2412 increased the circa zero-angle-of-attack (0.8°) lift coefficient by 42.4% compared to the 50% increase in camber. Thickness and maximum camber location had comparatively little effect on lift generation but influenced stall characteristics. These results provide practical insight into how isolated geometric modifications influence aerodynamic performance and may assist preliminary airfoil design before more detailed optimization studies are conducted.

Keywords: Airfoil optimization; Computational fluid dynamics (CFD); NACA airfoils; Lift coefficient analysis; Airfoil geometry effects; Aerodynamic performance; Reynolds number effects; Stall behavior

INTRODUCTION

Optimizing airfoils is an important process in aerodynamic design that advances the achievement of efficiency and environmental goals. Since airfoil optimization is meant to improve an airfoil's performance in a given niche, little attention has been given to the generalizable principles surrounding the matter aside from general aerodynamic theory. This method of optimization, now often employing AI and algorithms to evaluate hundreds or thousands of candidate airfoils, leaves little room for understanding how the subtle tweaks improve performance (1).

Current literature reflects this as well. Papers often focus on how a single aspect of an airfoil influences airflow behavior or on specific subsections of flight dynamics, rather than on generalizable conclusions.

Corresponding author: Patrick Louden, E-mail: plouden@eastsideprep.org.

Accepted August 4, 2026
https://doi.org/10.70251/HYJR2348.44788796

The literature available in the field, therefore, makes it difficult to extract a unified account of how specific variables can affect flight characteristics or does not contain takeaways that are meaningful beyond the small subsection of aerodynamics the paper directly addresses (2).

Simplified aerodynamic theory, particularly thin-airfoil theory, predicts that camber primarily modifies the zero-lift angle while preserving an approximately linear lift-curve slope of 2π per radian. The fact that it increases the lift coefficient of an airfoil at zero angle of attack, and that the general effect is an upward shift in the lift curve, is well established in classic aerodynamics (3). Practically, research is limited to discussing the implications of camber on specific airfoils, often focusing on the optimization of them (4). This structure does not establish a unified framework necessary to make claims about the global effects of camber on performance. The effects of camber on airflow and flow separation have also been examined, but the analyses emphasize specific, fixed states, leaving a lack of a comprehensive review of their effects across angles of attack or Reynolds numbers (5).

Thin airfoil theory cannot make claims about the influence of the point of maximum camber, as any location produces identical effects in this theory. Some practical studies have been conducted on airfoil thickness, but they primarily address stall behavior. Behavior has been noted, indicating that thinner airfoils are more prone to laminar separation bubble burst, triggering a leading-edge stall, while thicker airfoils demonstrate greater reverse flow over sections of the wing (6). The airfoils tested in this study were symmetrical, so the applicability to cambered airfoils is questionable. The majority of studies on airfoil thickness concern rotational dynamics, such as wind turbine blades, and were therefore not considered. Considering the location of maximum camber, the most relevant studies found triangular airfoils and hydrofoil cavitation. In the triangular airfoil study, no pattern between the point of maximum camber and the lift/drag ratio was identified across all the Reynolds numbers tested (7). The range tested was much lower than the range to be tested in this study. Hydrofoil cavitation can lend insights into flow separation and pressure gradients. That study found that the location of maximum camber at 35% of the chord length minimized the cavitation (8), indicating that this is the location in airfoils where flow separation is least likely to happen and pressure gradients are the most gradual.

Accordingly, the goal of this paper is to identify generalizable conclusions about the effects of isolated modifications to airfoil geometry on the lift generated by the airfoil. Establishing a theory, even a directional one, could aid in the understanding of concepts so often relegated to computer calculation and provide guidance for ideas on how to take a given starting airfoil and optimize it for a given Re. While high fidelity computer simulations remain the most accurate design approach, an intuitive understanding of these concepts is critical for streamlining engineering work. To accomplish this, this paper focused on the comparative analysis of airfoils with specific quantitative adjustments (e.g., camber, thickness, or the location of maximum camber), holding all else constant. The effects of these changes were measured through the coefficient of lift, defined in: $L = \frac{1}{2} \rho V^2 S C_L$. The coefficient is a factor introduced to compensate for discrepancies arising from different wing geometries or different angles of attack, producing a numerical representation of the performance of the wing in that specific configuration. Given that, this paper graphed the coefficient of lift and the angle of attack, normalizing the coefficient with respect to the angle of attack, allowing the full effects of the airfoil geometry to be isolated.

Another important consideration is that this paper examines only the 2D performance of airfoils. It does this through a quasi-2D method, where the bounding box spans only the length of the wingspan, leaving no space for airflow around the ends. This omission of wingtips prevents any negative or turbulent effects from interfering with the experiments conducted in this study. Therefore, any practical applications of the findings or real-world testing should expect underperformance of the specified quantities, as the airfoils tested here are considered to have an infinite aspect ratio. However, the study's effects are generalizable to the real world, as the airflow will still largely function as simulated.

Since computational fluid dynamics (CFD) was critical to the results of this paper, an introduction to it is prudent. The program used for all CFD simulations in this study is Ansys Fluent, an industry-standard tool well suited for moving-mesh and transient simulations (9,10). These features were used to allow airfoil movement while airflow continued, rather than running a steady-state calculation for each angle of attack. The way CFD arrives at the solution is by calculating error residuals from quantities such as momentum and energy at each time step (11). Once the residuals have converged to below a predetermined value (Fluent and this study use 10^{-3}), the progress on the next time step begins.

METHODS AND MATERIALS

The overall structure of the study consisted of testing four airfoils under four Reynolds numbers. Each simulation consisted of the airfoil smoothly moving from an angle of attack of 0 degrees to an angle of attack of 20 degrees over the course of 5 seconds.

Airfoils & NACA Standardization

The NACA standardization system for airfoils was used to ensure quantitative differences in airfoil geometry. The convention of the naming system is such: the first number represents the maximum camber as a percent of chord length, the second number represents the location of maximum camber in tens of a percent of chord length, while the last two digits represent the maximum thickness as a percent of chord length.

For this experiment, four different airfoils were tested. The NACA 2412 was chosen as the control airfoil because it is a commonly used profile and is prevalent in aerodynamic textbooks. To understand the implications of greater camber, the NACA 3412 was also tested. For the effects of airfoil thickness, the NACA 2406 was used. Finally, the NACA 2212 was tested to understand how the location of maximum camber impacts performance.

To create a model of each airfoil for the simulations, the "Aerofoil Script" plugin for Onshape was used. This plugin allows the user to specify the leading and trailing edges as points, along with all four digits of the NACA numbering convention. It will then generate a sketch of the side profile of said airfoil. For each airfoil, a 1.5 m chord and a 3 m span or a 7 m chord and 14 m span were used, depending on the tested Re. The bounding box of fluid extended 5 chord lengths away from the center of the wing in front, above, and below the airfoil. Behind the airfoil, the bounding box extended 7 chord lengths away from the center of the airfoil. These distances were chosen to allow all aerodynamic processes to occur without significant interference, while minimizing the volume being simulated.

Test Cases

To understand the implications of airfoil geometry across a variety of Re, four different test cases were established. These test cases were established as summarized in Table 1.

Rather than simulating different models for each test case, two different mesh sizes were used. The Reynolds number was kept constant, and the velocity was adjusted to counteract the size adjustment. Since the only data used from these tests are the coefficients of lift, not the raw lift force, this simplification has no impact, as the velocity will cancel out, and the observed behavior will remain consistent with the intended Re.

Even though the velocity some of the tests ran higher Mach numbers than are typically accepted for purely incompressible flow, since the CFD program used only incompressible models, this did not affect the quality of the data but rather mimicked the behavior of the airflow by running the test at the same Reynolds number that the test is intended to mimic. At 154.333 m/s, the airflow is at Mach 0.4535. At this speed, incompressible assumptions are only 0.7% off for pressure values, seen through comparing the compressible flow equation of pressure to Bernoulli's equation. Notably, this degree of disagreement is smaller than that found in the grid independence study. All tests were run with a viscosity of $1.7894 \cdot 10^{-5}$ kg/m·s and a density of 1.225 kg/m^3.

Simulations

Ansys Fluent was the CFD program used for this experiment. It was chosen for its ability to cope with large mesh changes during simulation. Each airfoil was imported into this program and meshed using the default

Table 1. Geometric and flow conditions for the four Reynolds-number test cases. *Intended and simulated chord lengths, inlet velocities, Reynolds numbers, and simulated Mach numbers are reported. All cases used air density of 1.225 kg/m³, dynamic viscosity of 1.7894×10^{-5} kg·m^{-1}·s^{-1}, and a continuous angle-of-attack sweep from 0° to 20° over 5 s.*

Intended Chord Length (m)	Intended velocity (m/s)	Reynolds Number	Simulated Chord Length (m)	Simulated Inlet Velocity (m/s)	Simulated Mach Number
0.5	30.8667	1,044,521	1.5	10.2889	0.0302
1.5	61.7333	6,267,127	1.5	61.7333	0.1814
3.0	154.333	31,335,568	7.0	66.1427	0.1943
7.0	154.333	73,116,483	7.0	154.3333	0.4535

settings. In Fluent, all default settings of version 26.1.0 with a pressure-based, transient solver were applied, except for the specified changes.

The velocity of the inlet and the airmass inside the volume (for initialization purposes) were set to the appropriate speed, yielding the desired Reynolds number of the test. The airfoil was given a motion profile that rotated it about its center at the appropriate angular velocity to move from a deflection of 0° to 20° in 5 seconds (ω = 0.0698132 rad/s). This gives a reduced frequency of 0.00508 for the Re = 1,044,521 tests, 0.00085 for the Re = 6,267,127 tests, 0.003694 for the Re = 31,335,568 tests, and 0.00158 for the Re = 73,116,483 tests. Since the greatest of these is only 0.005, an order of magnitude less than the upper barrier of what is considered quasi-steady state flow (12), this paper treated it as steady state. The walls were given the "deforming" characteristic, and mesh smoothing and remeshing were permitted. The remeshing criteria allowed a maximum cell skewness of 0.9 and face skewness of 0.7. The inlet and outlet sections were given "stationary" designations.

The simulation controls were as follows: up to 40 calculations per time step were allowed, but the residuals threshold was not adjusted; each time step was spaced by 0.1 seconds; 50 time steps were used in the simulation; and every second time step was saved. This yields 25 time steps per simulation for data and animations in post-processing; thus, this is the number of data points seen. Each data point therefore shows the airfoil at a deflection of 0.8° apart from adjacent time steps, starting at a deflection of 0.8° and ending at a deflection of 20°.

For the creation of animations of each test case, the scale was standardized by zooming into the center of the airfoil until the scale bar (at least in the viewing screen) showed a length of 3 m. A cut plane was used at 2.4 m, allowing the interior of the simulation to be viewed. The pressure contour was generated in 11 steps, with the maximum and minimum values consistent across all tests of the same Re and specified by examining the maximum and minimum pressures achieved in each Re, to ensure maximum visual detail. For the flow lines, 100 seed points were evenly spaced at the inlet and allowed to propagate through the simulation.

Some default settings should be noted, however. The turbulence model uses an SST k-ω model with a near-wall correlation and no laminar-to-turbulent transition model. Pressure-velocity coupling used a SIMPLE scheme. For special discretization, a least squares cell-based scheme was used for the gradient, a second order scheme was used for pressure, and a second order upwind scheme was used for momentum, turbulent kinetic energy, and specific dissipation rate. Temporal discretization used a first order implicit scheme. The inlet and outlet were designated as stationary, the walls as deforming, and the wing as a rigid body that rotated. All surfaces were assumed to be perfectly smooth, and the thermal condition was adiabatic. A standard initialization was used. A smooth transition was used for mesh inflation so no singular $^{y+}$ can be reported. An area average of y^+ was calculated, and all airfoils fell between $y^+ = 198$ and $y^+ = 243$. Inflation used a growth rate of 1.2, maximum layers of 25, and a transition ratio of 0.272. All generated meshes have a maximum of 25 layers with a 1.2 growth rate. The mesh is unstructured and contains 302,750 tetrahedrons. A grid independence study was conducted and found that comparing the performance between tetrahedral meshes of size 144,708, 405,494, and 618,743 with the original, the standard deviation of the C_L values between $\alpha = 0$ and α_{stall} averaged 2.85% of the value obtained using the mesh of 302,750 tetrahedrons. The average α_{stall} value across the four tested was 0.4° higher than the α_{stall} of the original case.

A time step independence study was also conducted. The standard time step used in the study was 0.1 seconds. Simulations were run with time steps of 0.05 seconds and 0.025 seconds. The standard deviation of the C_L values between $\alpha = 0$ and α_{stall} averaged 0.18% of the value obtained using the time step of 0.1 seconds. The α_{stall} value across all three cases was the same.

Although monitoring lift and drag per iteration to determine their convergence was not possible, every iteration of every simulation run did have the residuals monitored (continuity, x, y, and z velocities, k, and ω) and they converged below 10^{-3} between $\alpha = 0$ and α_{stall}. After α_{stall}, some time steps used all 40 allowed iterations without residuals converging due to the turbulent nature of the airflow. This was particularly common at α near 20°.

Data Processing

The lift force was defined as the force in the positive direction, defined as perpendicular to the chord of the airfoil when the angle of attack was 0°. The lift force and angle of attack of every time step were recorded and transferred into Excel, where the coefficient of lift was calculated using the surface area of the wing (1.5 m chord by 3 m span or 7 m chord by 14 m span, depending on the mesh), the velocity of the fluid, and the density of the fluid (1.225 kg/m^3). The coefficient of lift and angle of attack were then graphed and compared.

RESULTS AND DISCUSSION

As mentioned in the methods, the simulations yield 16 sets of coefficient of lift and angle of attack (α) data, comprising every combination of the four airfoils used in this experiment and the four Reynolds numbers explored. Because several attributes were explored, each will be examined individually, focusing on its raw effects and how it was affected by different Reynolds numbers. Since the dataset is structured around the NACA 2412 as the control airfoil, all comparisons of airfoils will be made against the NACA 2412 unless otherwise specified.

When discussing stall behavior in all following sections, stalls will be assumed to be exhibiting predominantly steady-state behavior. Given that the lowest reduced frequency of any test is $k = 0.00085$, above $k = 0.0001$, which was identified to give ideal static stall results, but below the threshold $k \approx 0.04$ where pronounced dynamic stalls begin, stalls in this study exhibit primarily static behavior (13). The study also found that delay increases with a power-law relationship rather than exhibiting a distinct transition between a dynamic and steady state stall. Therefore, although the airfoil is pitching and therefore formally unsteady, the low reduced frequency places it in a regime where only minor unsteady effects are expected. For this reason, all stall angles reported will come from the Re = 6,267,127, which is the case with the lowest reduced frequency of $k = 0.00085$.

Camber

Camber was examined using the NACA 3412 airfoil, which had 50% more camber than the control. The most noticeable difference was the increase in the zero angle of attack coefficient ($\alpha = 0$) of the lift value. Since no data was collected at exactly 0° α, the 0.8° α values will serve as a proxy. At those values, the NACA 3412 demonstrated, across all Re tested, an average $C_{L0} = 0.3271$, while the NACA 2412 averaged $C_{L0} = 0.2298$. This means that the NACA 3412 had a C_{L0} 42.4% higher than the NACA 2412, showing that the relative increase in camber between these two airfoils, holding all else constant, is roughly proportional to the increase in the C_{L0}. A notable area for future study would be to determine if there is a target C_{L0}, whether it is a reasonable approximation to take the current airfoil design and increase the camber by whatever factor is necessary to reach the desired performance. This application could be incredibly helpful, as it provides a close approximation for all αs near zero, making it easy to estimate changes to geometry needed for cruise optimization.

However, near the stall α, defined in this paper as the α at which the coefficient of lift was greatest, camber's effect no longer becomes as productive to greater lift generation. The NACA 3412 had a noticeably earlier stall angle, at 12°, while the NACA 2412 had a stall angle of 12.8°. Based on simulation data, the airflow over the top of the NACA 3412 is considerably faster in each simulation due to the greater curvature, making it more prone to turbulence. The maximum coefficient of lift achieved by each airfoil is slightly different, with the NACA 2412 averaging a maximum coefficient of lift across Re tested of 1.3797, only 4.6% lower than the NACA 3412. Because datapoints only exist every 0.8°, it is likely that the coarse nature of data plays a larger role in that difference than the airfoils themselves. Therefore, this increase in the camber should be interpreted as a translation of the coefficient of lift vs. angle of attack curve leftward rather than the typically conceived notion of upwards. This is consistent with the available data. Simple airfoils should have a coefficient of lift vs. angle of attack slope of roughly 2π, assuming the angle is in radians (3). Converting this to degrees and calculating what shift must be made to achieve the necessary increase in C_{L0} gives a leftwards shift of 1.03°, within the error of the 0.8° difference, due to datapoint resolution, in the stall angles of the airfoils.

The different Reynolds numbers had no measurable effect on the NACA 3412's performance relative to the control. It consistently had a roughly 1.42 times higher C_{L0} and stalled about a degree earlier. The only measurable difference was that it exhibited more turbulent behavior while stalled, defined as a greater variation of values in the datapoints after α_{stall} (Figure 1).

Thickness

The effects of the maximum thickness produced little difference. The airfoil tested for this aspect was the NACA 2406, so the insights can only be confidently generalized to reducing the thickness. The lift curves leading up to the stalling point are nearly identical, and only minor differences emerge at the stall point. The stall point is 0.8° earlier. Similar to the NACA 3412, the NACA 2406 exhibits highly turbulent stall behavior. This similarity leads to the conclusion that the greater an airfoil's curvature is over a given area, the more prone it is to stalling at lower angles of attack. Notably, the one Re in which the NACA 2406 outperformed the NACA 2412 was that with the lowest Reynolds number (1,044,521 Re). The coefficient of lift peaked noticeably higher here, reaching 1.4663, higher than any other airfoil during the Re = 1,044,521 tests and 16.33% higher than the maximum coefficient of lift of the NACA 2412 under the same Re (Figure 2).

Because of the sharper nose, the airflow acceleration is much more localized. This effect of a section of higher energy air improves the flow's ability to follow the surface's curvature. The low curvature outside of the nose section helps prevent trailing-edge flow separation. The NACA 2412, however, does not experience this. Its more gradual curve leads to the growing dominance of a trailing-edge stall, decreasing the coefficient of lift even though it has a later α_{stall} of α = 14.4° rather than α_{stall} = 13.6° for the NACA 2406. This effect is not observed in other Re, likely because the higher Reynolds numbers promote surface-following flow, but the increased turbulence increases the risk of leading-edge stall, which is what the NACA 2406 succumbs to (Figure 3).

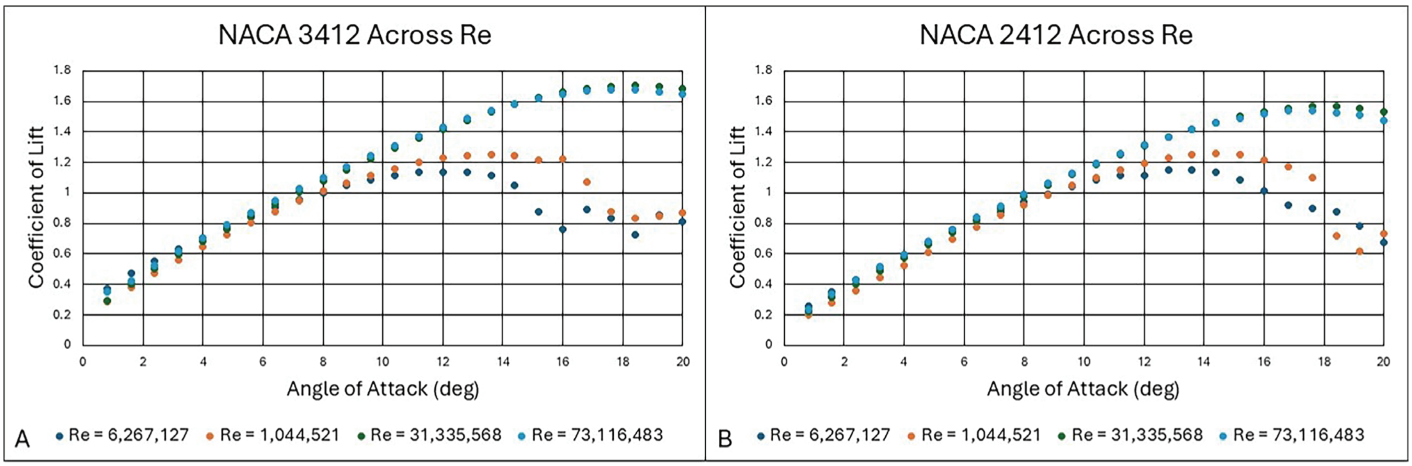

Figure 1. Effect of camber on lift across Reynolds-number test cases. *Transient, quasi-steady coefficient-of-lift (C_L) curves are shown as functions of angle of attack (α) for (A) the NACA 3412 airfoil and (B) the NACA 2412 control airfoil at Reynolds numbers (Re) of 1,044,521; 6,267,127; 31,335,568; and 73,116,483. In each simulation, the airfoil rotated continuously from 0° to 20° over 5 s, and data were recorded at 0.8° intervals beginning at 0.8°.*

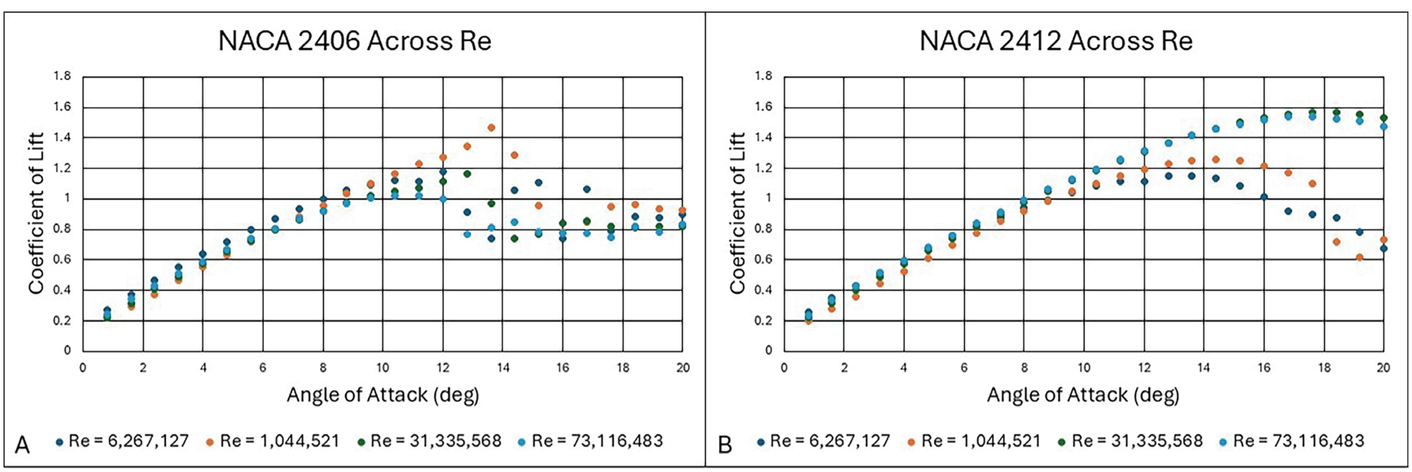

Figure 2. Effect of maximum thickness on lift across Reynolds-number test cases. *Transient, quasi-steady coefficient-of-lift (C_L) curves are shown as functions of angle of attack (α) for (A) the NACA 2406 airfoil and (B) the NACA 2412 control airfoil at Reynolds numbers (Re) of 1,044,521; 6,267,127; 31,335,568; and 73,116,483. The comparison isolates the effect of reducing maximum thickness from 12% to 6% of chord while maintaining the same maximum camber and camber location. Each simulation covered 0°–20° over 5 s, with data recorded every 0.8° beginning at 0.8°.*

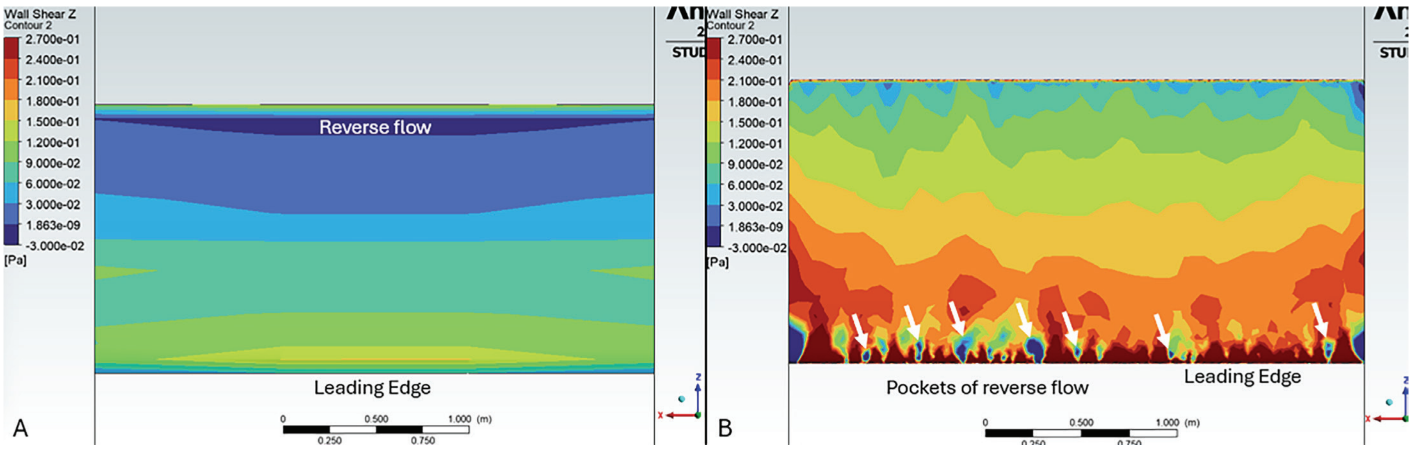

Figure 3. Initial reverse-flow locations for the NACA 2412 and NACA 2406 airfoils. *Wall-shear-stress contours from transient, quasi-steady pitching simulations at Re = 1,044,521 are shown for (A) the NACA 2412 airfoil at α = 16° and t = 4.0s, where reverse flow is observed near the trailing edge, and (B) the NACA 2406 airfoil at α = 12° and t = 3.0s, where reverse flow is observed near the leading edge.*

Because of this similarity in performance, the practical benefits and drawbacks primarily result from the direct consequences of the airfoil being thinner. The reduced frontal area and sharper nose cause this airfoil to have significantly less drag, only 29.02% of the NACA 2412's drag force at α = 0. Since the airfoil has a frontal thickness of half that of the NACA 2412 when at α = 0 due to the span of the NACA 2406 tested being identical to that of the NACA 2412 while the height of the NACA 2406 is half that of the NACA 2412. This indicates the coefficient of drag for a NACA 2406 at α = 0 is 58.04% that of the NACA 2412 under the same conditions. The potential drawback stems from the reduced interior area of the airfoil, meaning less room for flap mechanisms, control surface actuators, lights, and particularly fuel. The reduced interior volume also reduces the available space for structural components. Because of these benefits and drawbacks, aircraft that prioritize aerodynamic efficiency and a greater lift to drag ratio rather than fuel capacity, such as gliders, often employ such airfoils (14).

Position of Maximum Camber

The location of maximum camber was evaluated by comparing the NACA 2212, an airfoil with its position of maximum camber at 20% of its chord, rather than the 40% of chord possessed by the NACA 2412. Below is a table comparing the various attributes of the two different airfoils (Table 2).

The adjustment of the point of maximum camber had it underperforming in nearly every metric under the lower Reynolds numbers tested. C_{L0} was marginally lower, but the greatest difference was in the maximum coefficient of lift. As α increases, the coefficient of lift slowly grows further away from the NACA 2412's underperforming, in the 1.5 m mesh, it to greater and greater degrees. This, combined with the slightly earlier stalling behavior of the airfoil, contributes to the underperformance under those Re.

Under higher Re, the NACA 2212 achieved a higher C_{LMax} than the NACA 2412. The stall point for the NACA 2212 under these tests is slightly later, and it is important to remember that these tests have higher reduced

Table 2. *Comparison of lift coefficients and stall angles between the NACA 2412 and NACA 2212.*

Metric	NACA 2412	NACA 2212	Percent Difference
Average C_{L0}	0.2297	0.2156	6.16 %
Average C_{LMax} for 1.5 m mesh	1.2064	1.1186	7.27 %
Average C_{LMax} for 7 m mesh	1.5529	1.7310	11.47 %
α_{stall} (deg)	12.8	12	6.67 %

frequencies. However, no theory is proposed by this paper for why this behavior exists.

The reason the coefficient of lift starts underperforming is in exact opposition to why the NACA 2412 performed well: a blunter nose increases the likelihood of trailing-edge stalls. The blunter nose does not increase velocity quite as much. It has a more rounded leading edge than the NACA 2412, decreasing the likelihood of leading-edge stalls, but the nose section as a whole is more curved, increasing the likelihood of flow separation across these sections of the airfoil. The proposed hypothesis is that, for each Re, there exists an optimal location where the point of maximum camber is. If, during testing, an airfoil demonstrates leading-edge stalls, the point of maximum camber should be moved forward. On the contrary, if the airfoil demonstrates trailing-edge stalls earlier and to a greater degree than desired, then the point of maximum camber should be moved backward. Thereby, increased performance near the stall comes at the cost of more violent stall behavior.

CONCLUSION

This study identified the effects of three main aspects of airfoil geometry: camber, thickness, and the point of maximum camber. The camber of an airfoil improved the lift generation roughly proportional to the factor by which the camber was increased at low angles of attack when comparing the NACA 3412 to the NACA 2412. If this is generalizable, it could prove useful for optimizing airfoils at cruise, where a specific lift-generation target must be met, and the camber and angle of attack can be traded to maximize the lift-to-drag ratio. The thickness of an airfoil is largely a practical matter concerning internal volume and the drag it creates. While thickness does not significantly affect an airfoil's lift generation, it does significantly impact stall behavior. Finally, the point of maximum camber is a tradeoff between which stalling conditions are reached first. Points farther forward encourage trailing-edge stalls, while points farther aft encourage leading-edge stalls.

Based on the performance improvements desired by the engineering team, minor tweaks to the existing airfoil geometry can be made following these conclusions. However, these conclusions are far from perfect; the implications of combining several of these design tweaks are still unknown. Given the complex nature of fluid dynamics, it is likely that emergent properties arise from their combinations. Furthermore, the influence of the aspects was studied only in one direction from the control, so the effects in the other direction can be hypothesized but not established. These limitations naturally suggest opportunities for further research. This study could be extended to a collection of airfoils forming a three-dimensional parameter space structure around the NACA 2412, with the axes being camber, thickness, and the point of maximum camber. This experiment should also be conducted on more complex airfoils, such as supercritical airfoils, to determine how the same changes evoke different aerodynamic performance.

ACKNOWLEDGEMENTS

The author would like to thank Adam Kruger for his assistance in writing this paper and for providing valuable discussions and feedback throughout this project.

CONFLICT OF INTEREST

The author declares that there are no conflicts of interest related to this work.

REFERENCES

1. Xiong Z, Wang Y, Zhang P, Sun G, Chen Y, Lin J, *et al*. Learning to explain and quantify for aerodynamic prediction of airfoils. *Aerospace Science and Technology*. 2026; 178: 112417. doi:10.1016/j.ast.2026.112417
2. Skinner SN, Zare-Behtash H. State-of-the-art in aerodynamic shape optimisation methods. *Applied Soft Computing*. 2018 Jan 1; 62: 933–62. doi:10.1016/j.asoc.2017.09.030
3. Marchman JF. Chapter 3. Additional Aerodynamics Tools. In: Aerodynamics and Aircraft Performance [Internet]. Virginia Tech; 2021. Available from: https://pressbooks.lib.vt.edu/aerodynamics/chapter/chapter-3-additional-aerodynamic-tools/ (accessed on 2026-05-29)
4. Davari H, Davari M, Mihaela Botez R, Chowdhury H. Maximizing the Peak Lift-to-Drag Coefficient Ratio of Airfoils by Optimizing the Ratio of Thickness to the Camber of Airfoils. Sustainable Earth Review [Internet]. 2023 (accessed on 2026-05-29); 4 (3): 46–61. Available from: https://sustainearth.sbu.ac.ir/article_104402_4ac627768b005606375454e221e7e582.pdf
5. Karasu İ, Açikel HH, Koca K, Genç MS. Effects of Thickness and Camber Ratio on Flow Characteristics

over Airfoils. *Journal of Thermal Engineering*. 2020 Apr. 1; 6 (3): 242-5. doi:10.18186/thermal.710967

6. Sharma A, Visbal M. Numerical investigation of the effect of airfoil thickness on onset of dynamic stall. *Journal of Fluid Mechanics*. 2019 May; 870 (1): 870–900. doi:10.1017/jfm.2019.235
7. Henn A, Stameski K. Optimizing Max Camber Points Along Thin Triangular Airfoils for Higher Lift/Drag Ratios [Internet]. Embry-Riddle Aeronautical University Scholarly Commons; 2021. Available from: https://commons.erau.edu/aiaar2sc/2021/undergraduate/6/ (accessed on 2026-05-29).
8. Yang C, Tang F. Influence of Maximum Airfoil Camber Position on Hydrofoil Cavitation Performance. *Journal of Physics: Conference Series*. 2024 Oct 1; 2854 (1). doi:10.1088/1742-6596/2854/1/012033
9. Ansys Fluent Capabilities | Ansys [Internet]. Ansys. 2025. Available from: https://www.ansys.com/products/fluids/ansys-fluent/capabilities (accessed on 2026-07-13).
10. Scannell L. Dynamic Mesh Motion in Ansys Fluent [Internet]. SimuTech Group. 2025. Available from: https://simutechgroup.com/resources/blog/mesh-motion-parameters-in-ansys-fluent/ (accessed on 2026-07-13).
11. Versteeg HK, Malalasekera W. An Introduction to Computational Fluid Dynamics: The Finite Volume Method. Harlow: Pearson Education; 2007.
12. Leishman JG. Unsteady Aerodynamics, Aeroelasticity, & Flutter. In: Introduction to Aerospace Flight Vehicles [Internet]. Embry-Riddle Aeronautical University; 2023. Available from: https://eaglepubs.erau.edu/introductiontoaerospaceflightvehicles/chapter/unsteady-aerodynamics-flutter/ (accessed on 2026-07-13).
13. Le Fouest S, Deparday J, Mulleners K. The dynamics and timescales of static stall. *Journal of Fluids and Structures.* 2021 June 3; 104: 103304. doi:10.1016/j.jfluidstructs.2021.103304
14. Hall N. Lift to Drag (L/D) Ratio [Internet]. Glenn Research Center. NASA; 2021. Available from: https://www1.grc.nasa.gov/beginners-guide-to-aeronautics/lift-to-drag-l-d-ratio/ (accessed on 2026-07-13).